Kinetic mechanism and fidelity of nick sealing by *Escherichia coli* NAD$^+$-dependent DNA ligase (LigA)

Mathieu Chauleau and Stewart Shuman[*]

Molecular Biology Program, Sloan-Kettering Institute, New York, NY 10065, USA

ABSTRACT

Escherichia coli **DNA ligase (*Eco*LigA) repairs 3′-OH/5′-PO$_4$ nicks in duplex DNA via reaction of LigA with NAD$^+$ to form a covalent LigA-(lysyl-Nζ)–AMP intermediate (step 1); transfer of AMP to the nick 5′-PO$_4$ to form an AppDNA intermediate (step 2); and attack of the nick 3′-OH on AppDNA to form a 3′-5′ phosphodiester (step 3). A distinctive feature of *Eco*LigA is its stimulation by ammonium ion. Here we used rapid mix-quench methods to analyze the kinetic mechanism of single-turnover nick sealing by *Eco*LigA–AMP. For substrates with correctly base-paired 3′-OH/5′-PO$_4$ nicks, k_{step2} was fast (6.8–27 s^{-1}) and similar to k_{step3} (8.3–42 s^{-1}). Absent ammonium, k_{step2} and k_{step3} were 48-fold and 16-fold slower, respectively. *Eco*LigA was exquisitely sensitive to 3′-OH base mispairs and 3′ N:abasic lesions, which elicited 1000- to >20000-fold decrements in k_{step2}. The exception was the non-canonical 3′ A:oxoG configuration, which *Eco*LigA accepted as correctly paired for rapid sealing. These results underscore: (i) how *Eco*LigA requires proper positioning of the nick 3′ nucleoside for catalysis of 5′ adenylylation; and (ii) *Eco*LigA's potential to embed mutations during the repair of oxidative damage. *Eco*LigA was relatively tolerant of 5′-phosphate base mispairs and 5′ N:abasic lesions.**

INTRODUCTION

NAD$^+$-dependent DNA ligase (LigA) enzymes are ubiquitous in bacteria, where they are essential for growth and present attractive targets for anti-infective drug discovery (1). NAD$^+$-dependent ligases are encountered only sporadically outside the bacterial domain of life, e.g. in halophilic archaea and certain DNA viruses, and were probably acquired in these taxa by horizontal gene transfer (2–5). Archaea and eukarya rely on ATP-dependent DNA ligases for DNA replication and repair (6).

Escherichia coli DNA ligase (*Eco*LigA) is the founding member of the NAD$^+$-dependent DNA ligase family. *Eco*LigA seals 3′-OH/5′-PO$_4$ DNA nicks via three nucleotidyl transfer reactions. In step 1, LigA reacts with NAD$^+$ to form a covalent ligase-(lysyl^{115}-Nζ)–AMP intermediate and release NMN. In step 2, ligase–AMP binds to nicked DNA and transfers the adenylate to the 5′-PO$_4$ strand to form an adenylylated nicked intermediate, AppDNA. For step 3, LigA remains bound to the adenylylated nick and directs the attack of the 3′-OH on the 5′ phosphoanhydride linkage, resulting in a repaired phosphodiester and release of AMP (7–13). ATP-dependent ligases catalyze the identical chemistry during steps 2 and 3, but they use ATP as the substrate for ligase adenylylation during step 1 and release pyrophosphate.

The 671-aa *Eco*LigA protein consists of a catalytic core composed of a nucleotidyltransferase (NTase) domain (aa 70–316) and an OB-fold domain (aa 317–404). These two modules are common to NAD$^+$- and ATP-dependent DNA ligases (1). The LigA core is flanked by an N-terminal 'Ia' domain (aa 1–69) that confers NAD$^+$ specificity (2,5,14,15) and by three C-terminal modules: a tetracysteine Zn-finger domain (aa 405–432), a helix-hairpin-helix (HhH) domain (aa 433–586) and a BRCT domain (aa 587–671). Each step of the ligation pathway depends on a different subset of the LigA domain modules, with only the NTase domain being required for all steps. The crystal structure of *Eco*LigA bound to the nicked DNA-adenylate intermediate showed that the enzyme encircles the DNA helix as a C-shaped protein clamp (16). The protein-DNA interface entails extensive DNA contacts by the NTase, OB and HhH domains over a 19-bp segment of duplex DNA centered about the nick.

Structure-guided mutational analysis of *Eco*LigA has illuminated the contributions of the amino acid side chains that: (i) directly promote catalysis of one or more of the chemical steps in the ligation pathway; (ii) comprise the extended ligase-DNA footprint and make atomic contacts with the 3′-OH and 5′-phosphate strands or the continuous template strand; (iii) elicit conformational distortion of the DNA in the vicinity of the nick; and (iv) form or stabilize the ligase clamp (15,17–20). Similar comprehensive mutational analyses have been performed for an exemplary ATP-dependent DNA ligase (*Chlorella* virus DNA ligase; ChVLig), guided by the crystal structure of ChVLig-AMP bound to a 3′-OH/5′-PO$_4$ nick in duplex DNA (21–

---
[*]To whom correspondence should be addressed. Tel: +1 212 639 7145; Email: s-shuman@ski.mskcc.org

27), and for the ATP-dependent nick-sealing RNA ligase T4 Rnl2, informed by its crystal structure when bound to a 5′-adenylylated nicked intermediate (28–33).

A recent innovation in the functional analysis of ligases is the implementation of rapid mix-quench methods to study the transient-state kinetics of nick sealing by pre-formed ligase–adenylate. Single-turnover kinetic studies have been performed for *Chlorella* virus DNA ligase (25–27), human DNA ligase I (34), bacteriophage T4 DNA ligase (35) and T4 RNA ligase 2 (36).

Here, our goal was to explore the kinetic mechanism of *Eco*LigA, by analyzing the transient-state kinetics of nick sealing by pre-formed *Eco*LigA–AMP. After deriving rate constants for the 5′-adenylylation (step 2) and phosphodiester synthesis (step 3) reactions on a series of nicked substrates with all canonical base-pairs at the 3′-OH and 5′-PO$_4$ ends of the nick, we proceeded to gauge the effects of base mispairs and base damage at the nick 3′-OH and 5′-PO$_4$ terminus on the kinetics of nick sealing. Our studies provide new insights to ligase fidelity and the potential for ligase-mediated mutagenesis.

MATERIALS AND METHODS

Recombinant *Eco*LigA

LigA was produced in *E. coli* BL21(DE3) as an N-terminal His$_{10}$ fusion protein and purified from a soluble lysate of IPTG-induced cells by Ni-agarose chromatography as described (17). The 200 and 500 mM imidazole eluate fractions containing His$_{10}$*Eco*LigA were pooled (90 mg protein) and dialyzed against buffer containing 50 mM Tris–HCl (pH 7.5), 50 mM NaCl, 10% glycerol. Protein concentration was determined with the BioRad dye reagent using bovine serum albumin as the standard. The recombinant *Eco*LigA preparation comprises a mixture of ligase apoenzyme and ligase–adenylate intermediate. The concentration of *Eco*Lig–AMP was determined by measuring NAD$^+$-independent sealing of a singly nicked 36-bp substrate as a function of input *Eco*LigA, whereby there is a 1:1 correspondence between molar yield of ligated 36-mer and the molar amount of catalytically active *Eco*LigA–AMP in the reaction mixture. From the slope of the titration curve in the linear range of enzyme dependence, we determined that 20% of the total *Eco*LigA was pre-adenylylated and active in nick sealing.

To increase the extent of ligase pre-adenylation, we reacted the *Eco*LigA preparation with NAD$^+$ *in vitro*. A reaction mixture (100 ml) containing 50 mM Tris-HCl (pH 7.5), 5 mM DTT, 5 mM MgCl$_2$, 1 mM NAD$^+$ and 45 mg *Eco*LigA was incubated at 37°C for 1 h. The reaction was quenched by adjusting the mixture to 10 mM EDTA. The mixture was applied to a 5-ml DEAE-Sephacel column that had been equilibrated with buffer A (50 mM Tris-HCl, pH 7.5, 5 mM DTT, 2 mM EDTA, 10% glycerol) containing 50 mM NaCl. The column was washed with 20 ml of the same buffer and then eluted stepwise with 100, 200, 400 and 500 mM NaCl in buffer A. *Eco*LigA was recovered in the 200 and 400 mM NaCl eluate fractions, which were pooled (40 mg protein). Titration of the DEAE-Sephacel preparation for NAD$^+$-independent nick sealing showed that 80% of the total enzyme was *Eco*LigA–AMP. This enzyme preparation

was used for the transient-state kinetic analysis of nick sealing.

Nicked duplex substrates

Unmodified DNA oligonucleotides and DNAs containing single 8-oxoguanine or THF abasic nucleoside modifications were purchased from Eurofins MWG Operon. The pDNA strand was 5′ ^{32}P-labeled using T4 polynucleotide kinase and [γ^{32}P]ATP and then purified by electrophoresis through a non-denaturing 18% polyacrylamide gel. To form the nicked substrates, mixtures of pDNA strand, DNA$_{OH}$ strand and 36-mer complementary template strand were annealed at a molar ratio of 1:5:2 in 200 mM NaCl, 10 mM Tris-HCl (pH 8.0), 1 mM EDTA by heating for 1 min at 95°C, then cooling slowly to 22°C. The substrates were stored at –20°C and thawed on ice immediately prior to use.

Kinetics of single-turnover nick sealing

A Kintek RQF3 rapid chemical quench apparatus was used to assay the reaction of a ^{32}P-labeled nicked duplex with a 20-fold molar excess of *Eco*LigA–AMP at 22°C in the absence of added NAD$^+$, with reaction times in the range of 0.01 to 5 s. Longer reaction times were assayed manually. The reaction mixtures contained 50 mM Tris-HCl (pH 7.5), 5 mM DTT, 5 mM MgCl$_2$, 10 mM (NH$_4$)$_2$SO$_4$, 0.1 μM 5′ ^{32}P-nick-labeled DNA substrate and 2 μM *Eco*LigA–AMP. The rapid kinetic measurements were initiated by mixing two solutions (20 μl each) of 50 mM Tris-HCl (pH 7.5), 5 mM DTT, 10 mM MgCl$_2$, 10 mM (NH$_4$)$_2$SO$_4$, containing 0.2 μM nicked duplex substrate and 4 μM *Eco*LigA–AMP, respectively. The reactions were quenched by rapid mixing with 110 μl of 90% formamide, 40 mM EDTA. The products were analyzed by urea-PAGE, and the distribution of ^{32}P-labeled nucleic acids (as sealed 36-mer product, AppDNA intermediate and residual pDNA substrate) was quantified by scanning the gel with a Fujix BAS2500 imager. Experiments were repeated in triplicate. The distributions of AppDNA intermediate and sealed product were plotted as a function of reaction time. As noted previously for *Chlorella* virus DNA ligase (25) and T4 Rnl2 (36), our initial modeling of the data in Prism to a simple sequential reaction pathway described by two rate constants—for 5′-adenylylation (step 2) and phosphodiester synthesis (step 3)—yielded poor fits to the experimental kinetic profiles for the 5′-adenylylated intermediate, the level of which typically declined more slowly than could be simulated by the simple sequential pathway. To better model the experimental profiles for AppDNA and sealed product, we used the kinetic scheme described for *Chlorella* virus DNA ligase (25), which includes a reversible transition of the step 2 product from an active 'in pathway' state to an inactive 'out of pathway' state. Simulations and curve fitting to the experimental data to this model were performed in MATLAB by inputting an initial k_{step2} value (obtained by plotting the sum of AppDNA plus sealed DNA as a function of time and fitting the data to a single exponential in Prism) and stipulating that all other rates be greater than zero. Exemplary curve fits are shown in the figures. The step 2 and step 3 rate constants are compiled in the figures; the error values represent one standard deviation.

RESULTS AND DISCUSSION

Kinetics of nick sealing by *Eco*LigA

Rapid mix-quench methods have been applied to study the transient-state kinetics of nick sealing by ATP-dependent polynucleotide ligases (25–27,34–36). Here we extended this approach to the NAD$^+$-dependent DNA ligase *Eco*LigA. The substrates we employed were singly nicked duplexes composed of a DNA$_{OH}$ strand and a pDNA strand (labeled with ^{32}P at the nick 5′-PO$_4$) annealed to a 36-mer DNA template strand (Figure 1A). We initially varied the identity of the N:X base pair at the nick 5′-PO$_4$ end, as T:A, A:T, G:C or C:G. The nicked duplexes (0.1 μM) were reacted with a 20-fold molar excess of *Eco*LigA–AMP (2 μM) in the presence of 5 mM Mg^{2+} but in the absence of NAD$^+$. Omission of NAD$^+$ restricts the system to one round of catalysis of 5′ adenylylation (step 2) and phosphodiester formation (step 3). The reactions were quenched with EDTA and formamide and the products were analyzed by urea-PAGE. The use of a Kintek rapid mix-quench apparatus accessed the reaction on a millisecond time scale, which was necessary to observe the formation and intermediacy of the AppDNA species *en route* to the sealed 36-mer product (Figure 1A).

The AppDNA intermediate was evident at the earliest times sampled (10 or 20 ms) and it peaked—depending on the 5′ N:X base pair—at 50 ms (G:C; C:G), 100 ms (A:T) or 250 ms (T:A), at which times AppDNA comprised between 35% and 50% of the total labeled DNA. AppDNA decayed steadily thereafter as the sealed 36-mer DNA product accumulated (Figure 1A). For all four 5′ N:X substrates, the ligation reaction attained an endpoint by 2 s, with 92–94% of the input DNA being sealed. (The residual unreactive material reflects incomplete annealing of the three DNA strands that comprise the nicked duplex.)

The kinetic profiles were fit in MATLAB to a unidirectional scheme of 5′-PO$_4$ adenylylation (step 2: *Eco*LigA-AMP•pNick → *Eco*LigA•AppNick) and subsequent phosphodiester synthesis (step 3; *Eco*LigA•AppNick → *Eco*LigA•AMP•RNApDNA), with allowance for reversible branching of *Eco*LigA•AppNick to an 'out-of-pathway' state, as described in prior studies of *Chlorella* virus DNA ligase (25). The apparent step 2 and step 3 rate constants (k_{step2} and k_{step3}) for the series of correctly paired 5′ N:X nicks are tabulated in Figure 1B. The salient theme from the kinetic analysis is that rates of step 2 and step 3 are rapid and similar in magnitude (i.e. within a factor of two) for any given 5′ N:X substrate. The rate constants were similar for the 5′ A:T (k_{step2} = 27.0 s^{-1}, k_{step3} = 14.5 s^{-1}), 5′ G:C (k_{step2} = 20.5 s^{-1}, k_{step3} = 25.0 s^{-1}) and 5′ C:G (k_{step2} = 21.5 s^{-1}, k_{step3} = 41.0 s^{-1}) nicks, but slower for the 5′ T:A nick (k_{step2} = 6.8 s^{-1}, k_{step3} = 8.3 s^{-1}).
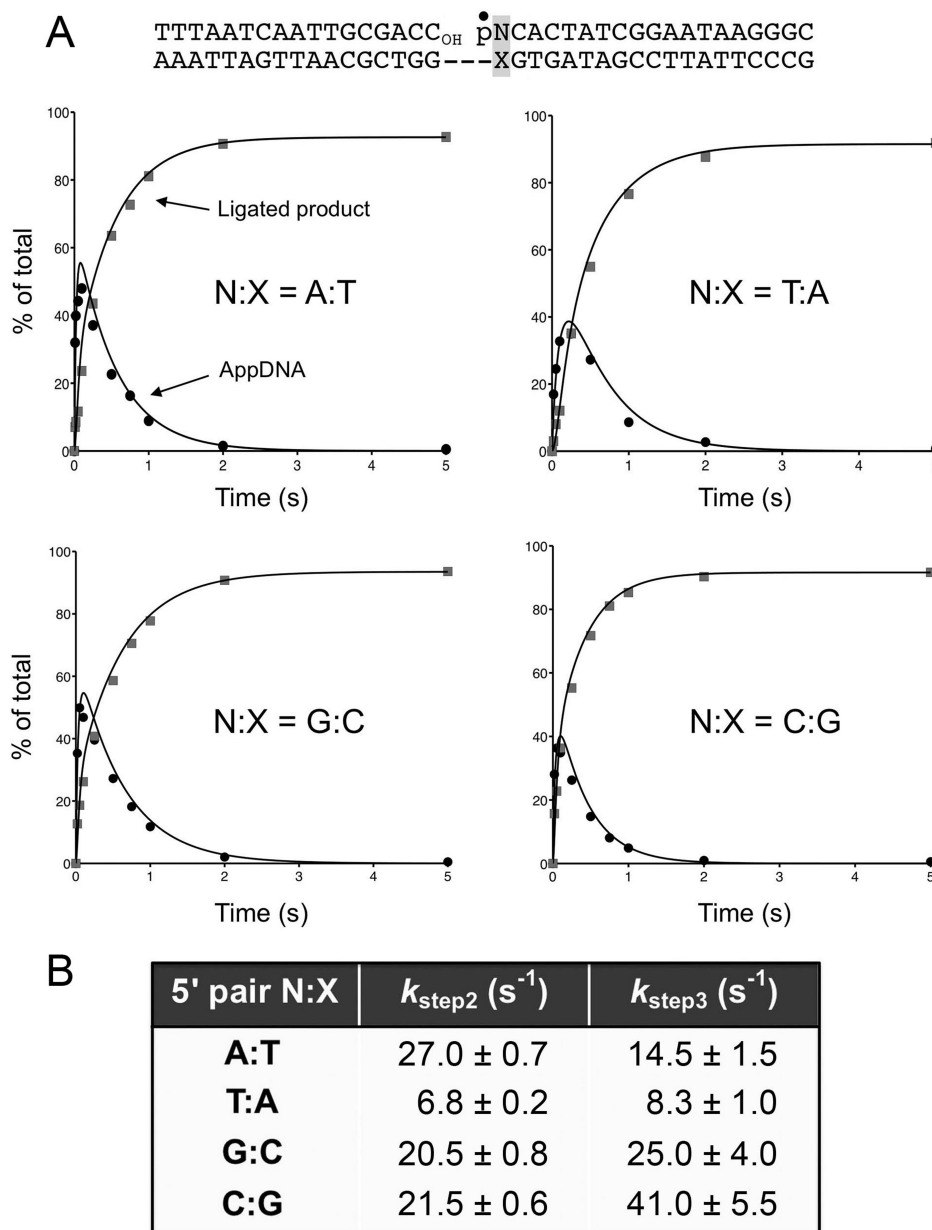
We extended the kinetic analysis to a series of singly nicked duplexes in which we varied the identity of the N:X base pair at the nick 3′-OH end, as T:A, A:T, G:C or C:G (Figure 2A). [Note that the DNA sequences flanking the nick are identical in the 5′ N:X and 3′ N:X substrates used in Figures 1 and 2, respectively; the position of the nick is shifted by one base pair to the left in Figure 2A compared to Figure 1A.] We again observed a precursor-product relationship between AppDNA and sealed DNA, with AppDNA peaking at early times (50 to 100 ms) and comprising between 26% and 39% of the total DNA (Figure 2A). The reactions attained or neared their endpoints by 2 s, with 95–96% of the input labeled 5′-PO$_4$ strand being sealed at the endpoints. The values for the rate constants of the reaction with the 3′ N:X substrates ranged from 9.2 s^{-1} to 22.6 s^{-1} for step 2 and 23.5 s^{-1} to 42.0 s^{-1} for step 3 (Figure 2B).

It is instructive to compare the results for *Eco*LigA with the kinetic parameters for single-turnover sealing of DNA nicks by ATP-dependent DNA ligases. The observed step 2 and step 3 rate constants for *Chlorella* virus DNA ligase (ChVLig) were 2.4 s^{-1} and 25 s^{-1}, respectively (26,27). Thus, for ChVLig the attack of the nick 3′-OH on AppDNA is an order of magnitude faster than the formation of AppDNA. Similar single-turnover kinetic studies were reported for human DNA ligase I (k_{step2} 2.6 s^{-1}; k_{step3} 12 s^{-1}) (34) and T4 DNA ligase (k_{step2} 5.3 s^{-1}; k_{step3} 38 s^{-1}) (35). It would appear that diverse ATP-dependent DNA ligases have similar kinetic properties with respect to steps 2 and 3, whereby step 2 is rate limiting. By contrast, *Eco*LigA catalysis of step 2 is faster than that of ATP-dependent DNA ligases and is not disproportionate to the step 3 rate for most of the substrates tested. (Only the 3′ A:T and G:C nicks displayed a >2-fold difference between k_{step2} and k_{step3}.)

Effect of ammonium ion on the kinetics of *Eco*LigA nick sealing

*Eco*LigA reactions routinely include 10 mM ammonium sulfate, in light of the 'classic' findings of Modrich and Lehman, who reported in 1973 that the steady-state rate of sealing by *Eco*LigA was enhanced (up to 20-fold) by low concentrations of ammonium ion, whereas sealing by ATP-dependent T4 DNA ligase was unaffected by NH$_4^+$ (37). They found no effect of ammonium on the exchange reaction of LigA with NAD$^+$ and NMN and therefore concluded that activation by ammonium occurs at a step subsequent to formation of the LigA–AMP intermediate. We revisited this fascinating effect by analyzing the kinetics of single-turnover sealing of the nicked 3′ A:T duplex by *Eco*LigA–AMP in the absence of ammonium sulfate (Figure 3A). AppDNA comprised 12% of total DNA at 1 s. Sealed DNA accumulated steadily up to 10 s and attained an endpoint thereafter with 95% ligation (Figure 3A). The apparent rate constants were: k_{step2} = 0.33 ± 0.03 s^{-1} and k_{step3} = 2.62 ± 0.21 s^{-1}. Thus, a comparison with the kinetic data for the nicked 3′ A:T substrate in Figure 2 (k_{step2} = 15.9 ± 0.5 s^{-1} and k_{step3} = 41.9 ± 5.4 s^{-1}.) showed that 10 mM ammonium sulfate elicited a 48-fold increase in the rate of DNA adenylylation and a 16-fold increase in the rate of phosphodiester synthesis. A single-turnover kinetic analysis performed in the presence of 20 mM ammonium chloride (i.e. the same concentration of ammonium ion as 10 mM ammonium sulfate) revealed apparent rate constants k_{step2} = 8.2 ± 0.22 s^{-1} and k_{step3} = 20.7 ± 2.4 s^{-1}, signifying rate enhancements of 25-fold and 8-fold, respectively, compared to the no ammonium reaction.

A

```
TTTAATCAATTGCGACC_OH  pNCACTATCGGAATAAGGGC
AAATTAGTTAACGCTGG---XGTGATAGCCTTATTCCCG
```


B

| 5' pair N:X	k_{step2} (s^{-1})	k_{step3} (s^{-1})
A:T	27.0 ± 0.7	14.5 ± 1.5
T:A	6.8 ± 0.2	8.3 ± 1.0
G:C	20.5 ± 0.8	25.0 ± 4.0
C:G	21.5 ± 0.6	41.0 ± 5.5

Figure 1. Kinetics of single-turnover nick sealing by *Eco*LigA at correctly paired 5′-phosphate ends. (**A**) The singly nicked duplex substrate is shown with the 5′ ^{32}P-label at the nick denoted by ●. The 5′ N:X base pair at the nick (highlighted in the shaded box) is variable. The distributions of radiolabeled AppDNA intermediate (black circles) and sealed 36-mer DNA product (gray squares) during the reaction of *Eco*LigA–AMP at the indicated 5′ N:X nicks are plotted as a function of time. The curve fits to the kinetic scheme are shown. (**B**) The step 2 and step 3 rate constants for sealing nicks with the indicated 5′ N:X pairs are shown.

We proceeded to gauge the kinetics of single-turnover nick sealing as a function of ammonium sulfate concentration. These experiments revealed a linear increase in the step 2 rate constant between 0 and 10 mM ammonium sulfate. The step 2 rate of 17.6 ± 0.47 s^{-1} at 15 mM ammonium sulfate was 53-fold faster than that in the absence of ammonium (Figure 3B). The step 3 rate constant rose in a sigmodial fashion between 0 and 15 mM ammonium sulfate (Figure 3C), at which point k_{step3} was 54 ± 6.7 s^{-1} (20-fold greater than in the absence of ammonium sulfate).

*Eco*LigA fidelity: effect of 5′ base mispairs on the kinetics of nick sealing

Fidelity refers to the capacity of a ligase to discriminate in the sealing of substrates containing paired versus mispaired bases flanking the nick. Different DNA ligases display distinct patterns of fidelity, with respect to how well the ligase discriminates and the hierarchy of which mispairs are or are not accepted by the ligase (38–49). Here we evaluated the fidelity of *Eco*LigA, focusing first on the effects of 5′-PO$_4$ base mispairs on the transient state kinetics of nick sealing. Exemplary kinetic profiles for sealing of two 5′ N:purine
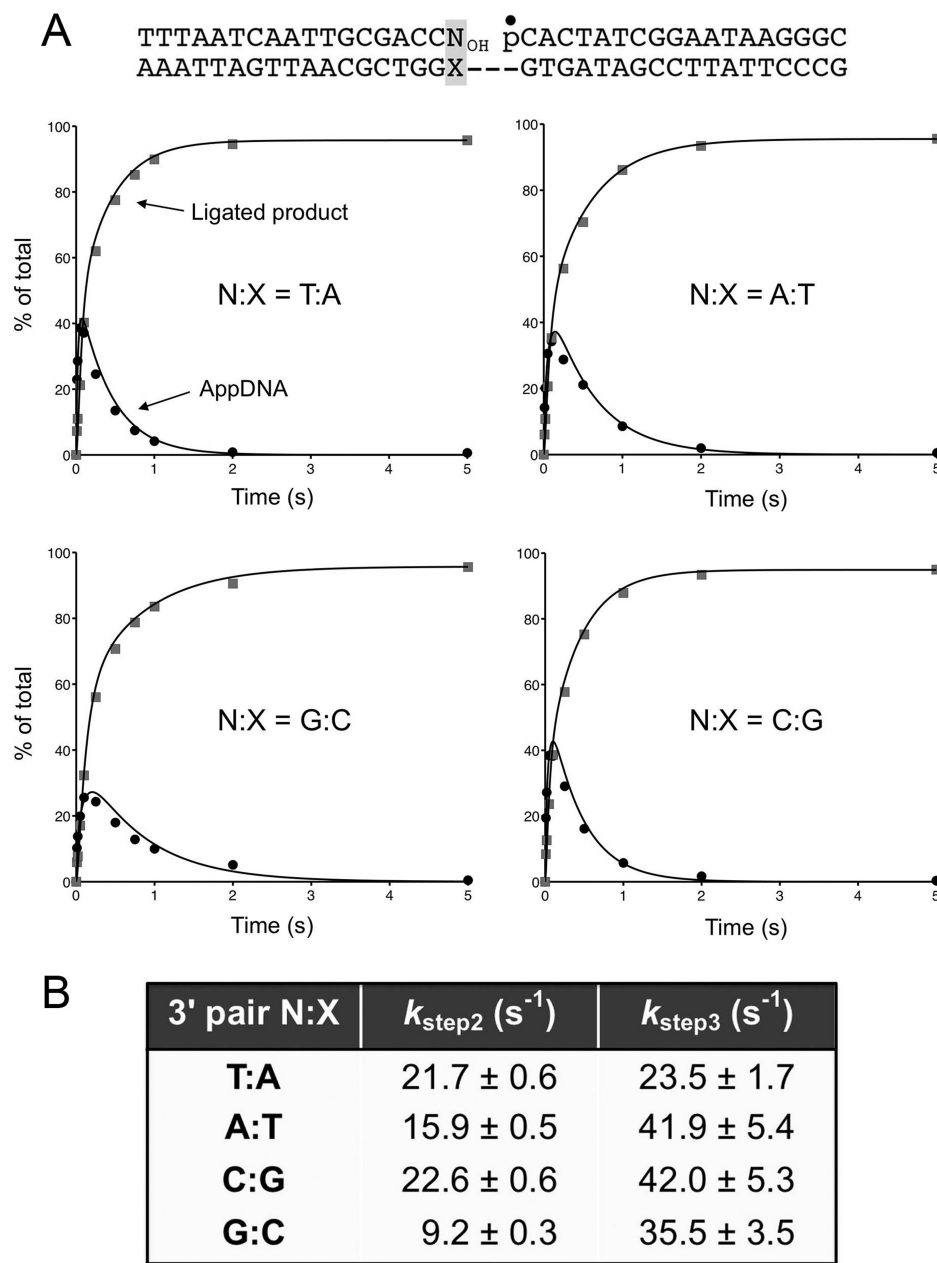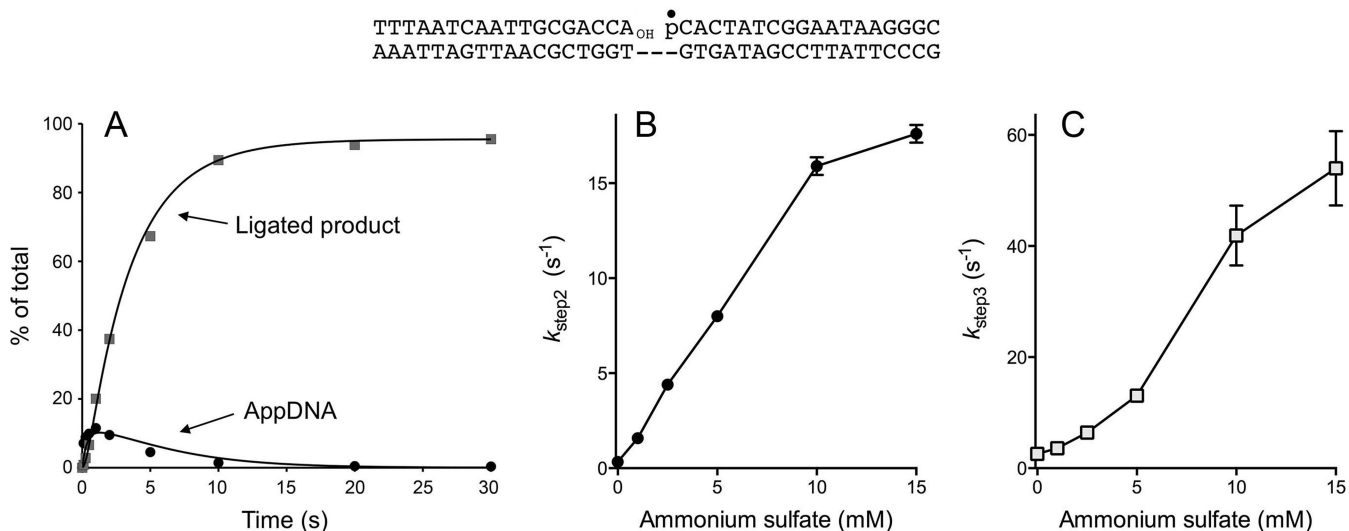
Figure 2. Kinetics of nick sealing by *Eco*LigA at correctly paired 3′-OH ends. (**A**) The singly nicked duplex substrate is shown with the 5′ ^{32}P-label at the nick denoted by ●. The 3′ N:X base pair at the nick (highlighted in the shaded box) is variable. The distributions of radiolabeled AppDNA intermediate (black circles) and sealed 36-mer DNA product (gray squares) during the reaction of EcoLigA–AMP at the indicated 3′ N:X nicks are plotted as a function of time. The curve fits to the kinetic scheme are shown. (**B**) The step 2 and step 3 rate constants for sealing nicks with the indicated 3′ N:X pairs are shown.

mispaired nicks (5′ C:A and 5′ G:G) are shown in Figure 4A,B; the rates constants for all 5′ N:X substrates are tabulated in Figure 4C.
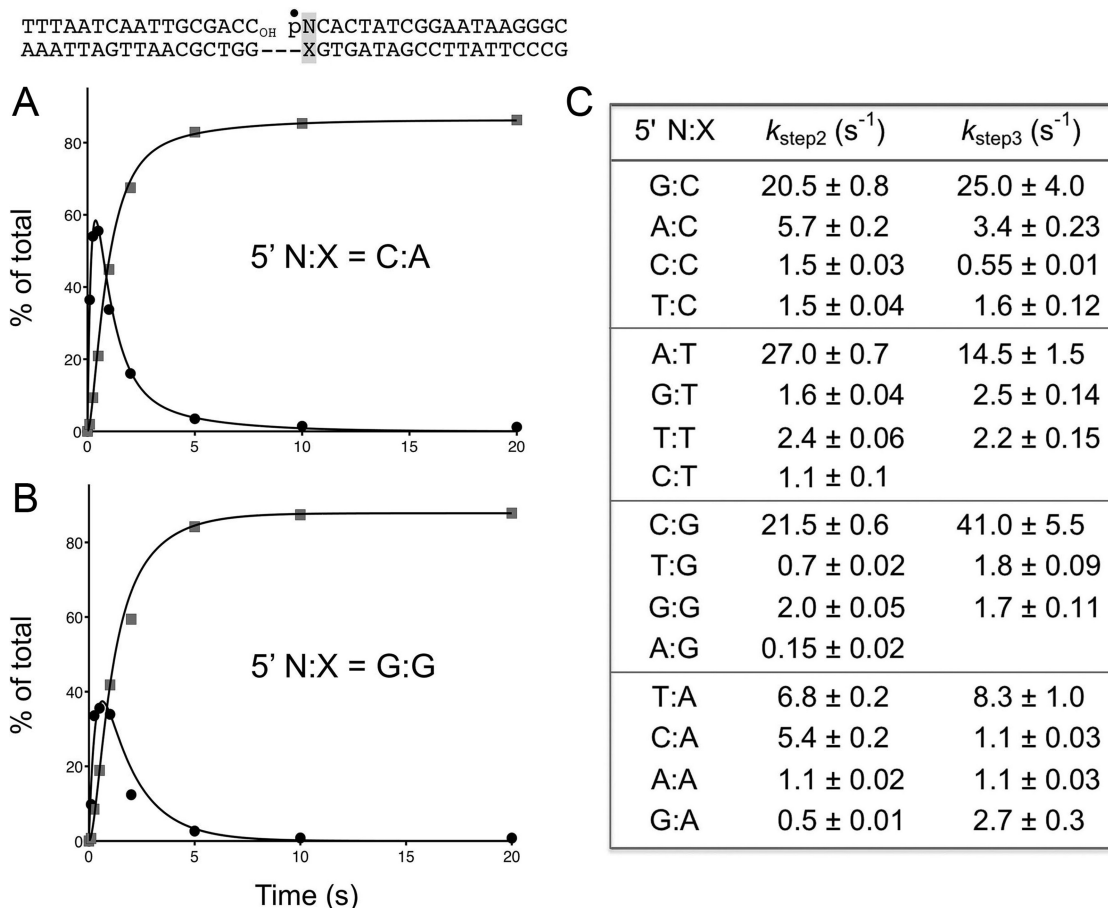
The step 2 rate constant of 5.4 s^{-1} for sealing the 3′ C:A mispair was close to the k_{step2} value of 6.8 s^{-1} for a correctly paired 5′ T:A nick; however the k_{step3} for the 5′ C:A mispaired nick of 1.1 s^{-1} was 7-fold lower than k_{step3} for the 5′ T:A paired nick. Thus, the 5′ C:A mispair exerted a greater impact on phosphodiester synthesis than on the preceding step of 5′ adenylylation. Whereas the 5′ A:A mispair

slowed both steps to 1.1 s^{-1}, the 5′ G:A mispair exerted a greater effect on step 2 (0.5 s^{-1}) than step 3 (2.7 s^{-1}).

The component rates of sealing of the 5′ G:G mispaired nick (k_{step2} 2.0 s^{-1}; k_{step3} 1.7 s^{-1}) were 11-fold and 24-fold slower than the rates for the correctly paired 5′ C:G nick (Figure 4C). The 5′ T:G mispair had a similar impact on k_{step3} (1.8 s^{-1}) and an even greater effect on k_{step2} (0.7 s^{-1}). The kinetic profile for the 5′ A:G mispair could not be used to determine a step 3 rate, insofar as AppDNA accumulated to an extent of 9% of total labeled DNA at 2 to 20 s and did not decline, even as ligated DNA increased steadily from

```
TTTAATCAATTGCGACCA_OH  •pCACTATCGGAATAAGGGC
AAATTAGTTAACGCTGGT---GTGATAGCCTTATTCCCG
```


Figure 3. Effect of ammonium ion on the kinetics of *Eco*LigA nick sealing. The singly nicked duplex substrate is shown with the 5′ ^{32}P-label at the nick denoted by •. (**A**) The distributions of radiolabeled AppDNA intermediate (black circles) and sealed 36-mer DNA product (gray squares) during the reaction of *Eco*LigA–AMP with the nicked DNA in the absence of ammonium sulfate are plotted as a function of time. The curve fits to the kinetic scheme are shown. (**B** and **C**) Single-turnover nick sealing was assayed in the presence of the indicated concentrations of ammonium sulfate. The apparent step 2 and step 3 rate constants (± standard error) are plotted as a function of ammonium sulfate concentration in panels B and C, respectively.

```
TTTAATCAATTGCGACC_OH  •pNCACTATCGGAATAAGGGC
AAATTAGTTAACGCTGG---XGTGATAGCCTTATTCCCG
```


5' N:X	k_{step2} (s^{-1})	k_{step3} (s^{-1})
G:C	20.5 ± 0.8	25.0 ± 4.0
A:C	5.7 ± 0.2	3.4 ± 0.23
C:C	1.5 ± 0.03	0.55 ± 0.01
T:C	1.5 ± 0.04	1.6 ± 0.12
A:T	27.0 ± 0.7	14.5 ± 1.5
G:T	1.6 ± 0.04	2.5 ± 0.14
T:T	2.4 ± 0.06	2.2 ± 0.15
C:T	1.1 ± 0.1	
C:G	21.5 ± 0.6	41.0 ± 5.5
T:G	0.7 ± 0.02	1.8 ± 0.09
G:G	2.0 ± 0.05	1.7 ± 0.11
A:G	0.15 ± 0.02	
T:A	6.8 ± 0.2	8.3 ± 1.0
C:A	5.4 ± 0.2	1.1 ± 0.03
A:A	1.1 ± 0.02	1.1 ± 0.03
G:A	0.5 ± 0.01	2.7 ± 0.3

Figure 4. Effects of 5′ N:X mispairs on the kinetics of nick sealing. The singly nicked duplex substrate is shown at the *top* with the 5′ ^{32}P-label at the nick denoted by •. The 5′ N:X site at the nick (highlighted in the shaded box) is variable. (**A** and **B**) The distributions of radiolabeled AppDNA intermediate (black circles) and ligated 36-mer DNA product (gray squares) during the reaction of *Eco*LigA–AMP at the 5′ C:A nick (panel A) and the 5′ G:G nick (panel B) are plotted as a function of time. The curve fits to the kinetic scheme are shown. (**C**) The step 2 and step 3 rate constants for sealing nicks with the indicated 5′ N:X configurations are shown.

7% at 2 s to 56% at 20 s. However, by plotting the sum of AppDNA plus ligated DNA as a function of time, as fitting the data to a single exponential, we obtained a k_{step2} value of 0.15 s^{-1} for the 5′ A:G mispair, which was 140-fold slower than k_{step2} for the correctly paired 5′ C:G nick.

The rate constants for sealing a 5′ A:C mispaired nick (k_{step2} 5.7 s^{-1}; k_{step3} 3.4 s^{-1}) were ≈4-fold and 7-fold slower than the rates for the correctly paired 5′ G:C nick. The k_{step2} values of 1.5 s^{-1} for the 5′ T:C and 5′ C:C mispairs were 14-fold slower; their k_{step3} values of 1.6 s^{-1} for 5′ T:C and 0.55 s^{-1} for 5′ C:C were 16-fold and 45-fold slower, respectively, than the paired 5′ G:C nick.

The 5′ G:T (k_{step2} 1.6 s^{-1}; k_{step3} 2.5 s^{-1}) and 5′ T:T (k_{step2} 2.4 s^{-1}; k_{step3} 2.2 s^{-1}) mispairs exerted similar slowing effects on 5′ adenylylation (17-fold and 11-fold, respectively) and phosphodiester synthesis (6-fold and 7-fold, respectively) compared with the 5′ A:T substrate. The kinetic profile for the 5′ C:T mispair was not suitable to derive a step 3 rate. AppDNA peaked at 38% of total labeled DNA at 1 s and declined to an endpoint value of 13% at 10 to 20 s. Ligated DNA comprised 22% of total at 1 s and reached an endpoint value of 70% at 20 s. The persistence of a residual AppDNA fraction that did not proceed through ligation is consistent with *Eco*LigA dissociation from said fraction of the mispaired 5′ AppC– nick termini after step 2 catalysis. Yet, by fitting the sum of AppDNA plus ligated DNA versus time to a single exponential, we obtained a k_{step2} value of 1.1 s^{-1} for the 5′ C:T mispair, which was 25-fold slower than k_{step2} for the correctly paired 5′ A:T nick.

Effect of 3′ base mispairs on the kinetics of nick sealing

The effects of 3′-OH base mispairs on ligation kinetics were uniformly more severe than the equivalent 5′ mispairs. Exemplary kinetic profiles for sealing four of the 3′ mispaired nicks (3′ A:A, 3′ C:A, 3′ G:T and 3′ T:G) are shown in Figure 5A–D, where the x-axis scales are in minutes rather than seconds as in the preceding experiments. Each graph includes separate plots of the levels of AppDNA, ligated DNA and the sum of AppDNA plus ligated DNA. In no case could the data be fit adequately to the kinetic scheme used above to derive step 2 and step 3 rate constants. In the case of the 3′ A:A mispair in Figure 5A, AppDNA accumulated steadily over 15 min and plateaued at 20–30 min, comprising 74% of the total DNA. Yet, there was scant formation of ligated product, which comprised only 8% of total DNA at 30 min. Clearly, the 3′ A:A mispair exerted a much stronger effect on step 3 than on step 2. Fitting of the sum of AppDNA plus ligated DNA to a single exponential (the curve fit to the open circles in Figure 5A) yielded a k_{step2} of 0.002 s^{-1} for the 3′ A:A mispair, which is four orders of magnitude slower that the step 2 rate at a paired 3′ T:A nick (see data complied in Figure 5E) and 550-fold slower than the step 2 rate at a 5′ A:A mispair (Figure 4).

The 3′ T:G mispair elicited a very different outcome, insofar as the ligated DNA accumulated steadily over 4 min and plateaued at 6–10 min, comprising 79% of the total DNA (Figure 5E). AppDNA comprised 6–8% of total DNA at 1–10 min. This kinetic profile indicated that the 3′ T:G mispair had a relatively greater effect on step 2 than on step 3. Fit-

ting AppDNA plus ligated DNA to a single exponential revealed a k_{step2} of 0.008 s^{-1} for the 3′ T:G mispair. This value which is 2800-fold slower than k_{step2} at a paired 3′ C:G nick (Figure 5E) and 90-fold slower than the step 2 rate at a 5′ T:G mispair (Figure 4).

The kinetic profiles for sealing of the 3′ C:A (Figure 5B) and 3′ G:T (Figure 5C) mispaired nicks reflected a 'middle-ground' between the extremes of 3′ A:A and 3′ T:G, insofar as: (i) AppDNA accumulated to high levels initially (50% at 6–15 min for 3′ C:A; 43–46% at 4–8 min for 3′ C:A) before declining gradually (to 34% for 3′ C:A: and 14% for 3′ G:T at 40 min); and (ii) ligated DNA product accumulated steadily and slowly (50% for 3′ C:A: and 77% for 3′ G:T at 40 min). By fitting AppDNA plus ligated DNA to a single exponential, we derived k_{step2} of 0.003 s^{-1} for the 3′ C:A mispair (7200-fold slower than k_{step2} at a paired 3′ T:A nick) and 0.006 s^{-1} for the 3′ G:T nick (2600-fold slower than k_{step2} at a paired 3′ A:T nick) (Figure 5E).

The step 2 rates for six other 3′ N:X mispairs (compiled in Figure 5E) highlight effects similar to those discussed above. To wit, k_{step2} values for 3′ T:C (0.009 s^{-1}), 3′ A:C (0.003 s^{-1}) and 3′ C:C (0.001 s^{-1}) nicks were 1000-fold, 3000-fold and 9200-fold slower than k_{step2} at a paired 3′ G:C nick. The k_{step2} values for 3′ C:T (0.012 s^{-1}) and 3′ T:T (0.003 s^{-1}) nicks were 1300-fold and 4000-fold slower than k_{step2} at a paired 3′ A:T nick. The k_{step2} of 0.001 s^{-1} for the 3′ G:G mispaired nick was 22600-fold slower than k_{step2} at a paired 3′ C:G nick.

Finally, two of the 3′ purine:purine mispairs, 3′ A:G and 3′ G:A, were inactive as substrates (Figure 5E), by the criterion than there was no detectable formation of AppDNA or ligated DNA during a 40 min reaction with *Eco*LigA–AMP.

Effects of 5′ and 3′ N:abasic sites on the kinetics of nick sealing

Abasic sites formed during base excision repair are among the most common DNA lesions and represent a challenge to genome integrity, e.g. by causing polymerases to stall, slip or misincorporate at an abasic site in the template strand. How nick-sealing ligases contend with abasic sites in the template strand has received scant attention. In a previous study, we reported the effects of 3′ N:abasic sites flanking the nick on the kinetics of single-turnover nick sealing by T4 RNA ligase 2 (36). Here we extended the kinetic analysis of *Eco*LigA to the sealing of nicked duplexes with THF (tetrahydrofuran) abasic sites in the template strand opposite the 5′-phosphate or 3′-OH deoxynucleotides at the nick. All N:abasic configurations were tested. We envisioned that comparison of the rate constants for N:abasic nicks to those of the correctly paired N:X substrates, and to N:X mispairs, would reveal, and potentially distinguish, effects of having no base pairing to template at the nick *versus* effects of mispairing.

The kinetic profiles for sealing of the 5 A:abasic and 5′ C:abasic substrates are shown in Figure 6A,B; the kinetic parameters for all four 5′ N:abasic substrates are compiled in Figure 6C. The step 2 and step 3 rate constants for the 5′ A:abasic (k_{step2} 3.9 s^{-1}; k_{step3} 2.6 s^{-1}), G:abasic (k_{step2} 4.4 s^{-1}; k_{step3} 2.2 s^{-1}), 5′ C:abasic (k_{step2} 1.5 s^{-1}; k_{step3} 0.8 s^{-1})
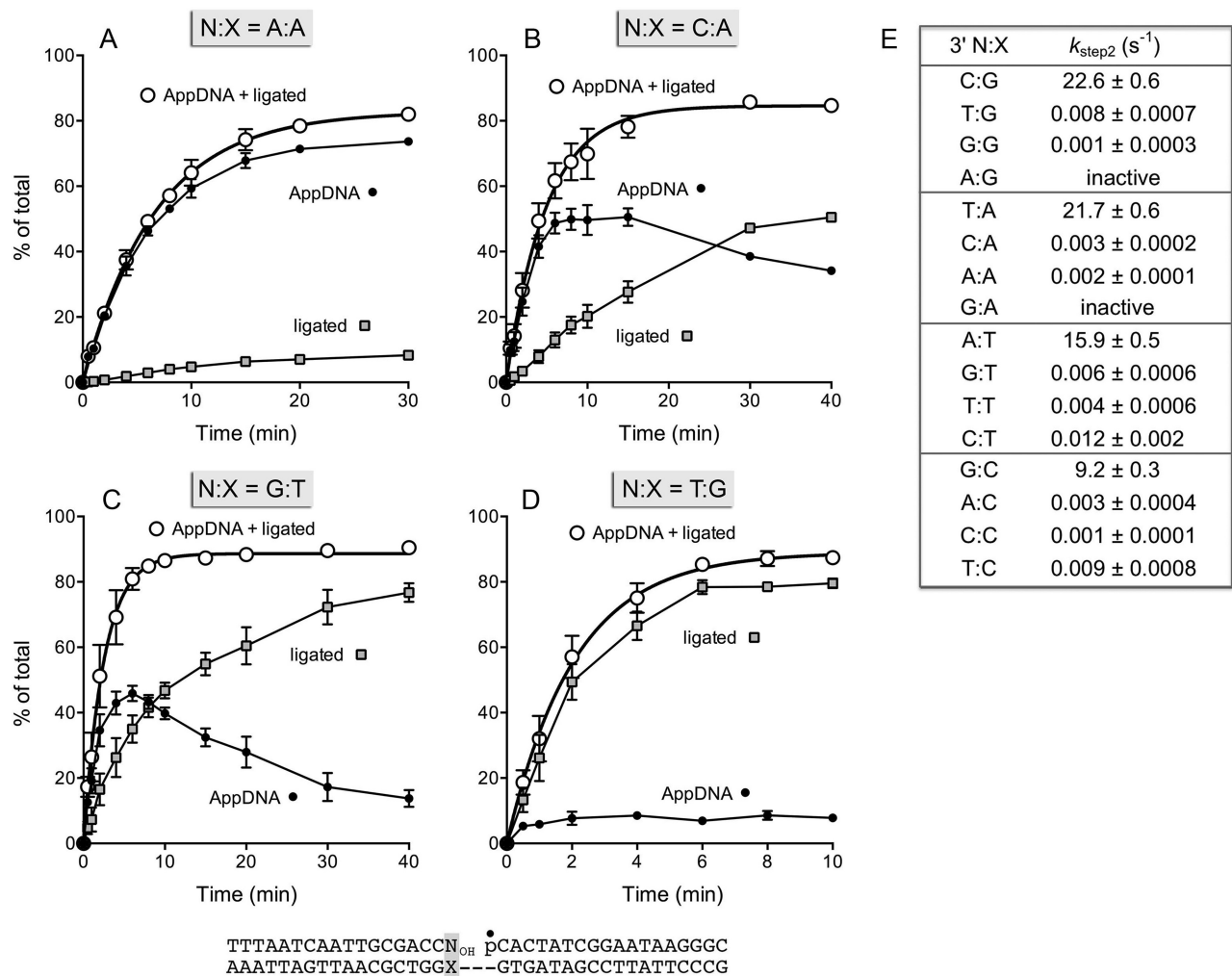
Figure 5. Effects of 3′ N:X mispairs on the kinetics of nick sealing. The singly nicked duplex substrate is shown at the *bottom* with the 5′ ^{32}P-label at the nick denoted by ●. The 3′ N:X site at the nick (highlighted in the shaded box) is variable. (**A–D**) The distributions (±SEM) of radiolabeled AppDNA intermediate (black circles), ligated 36-mer DNA product (gray squares) and the sum of AppDNA plus ligated DNA (open circles) during the reaction of *Eco*LigA–AMP at the indicated 3′ N:X mispaired nicks are plotted as a function of time. The thick black curves though the open circles show the nonlinear regression fits of the sum of AppDNA plus ligated DNA to a single exponential, from which we derived k_{step2}. (**E**) The step 2 rate constants for sealing nicks with the indicated 3′ N:X configurations are shown. The 3′ A:G and 3′ G:A mispaired nicks were deemed inactive as substrates, by the criterion than there was no detectable formation of AppDNA or ligated DNA during a 40 min reaction with *Eco*LigA–AMP.
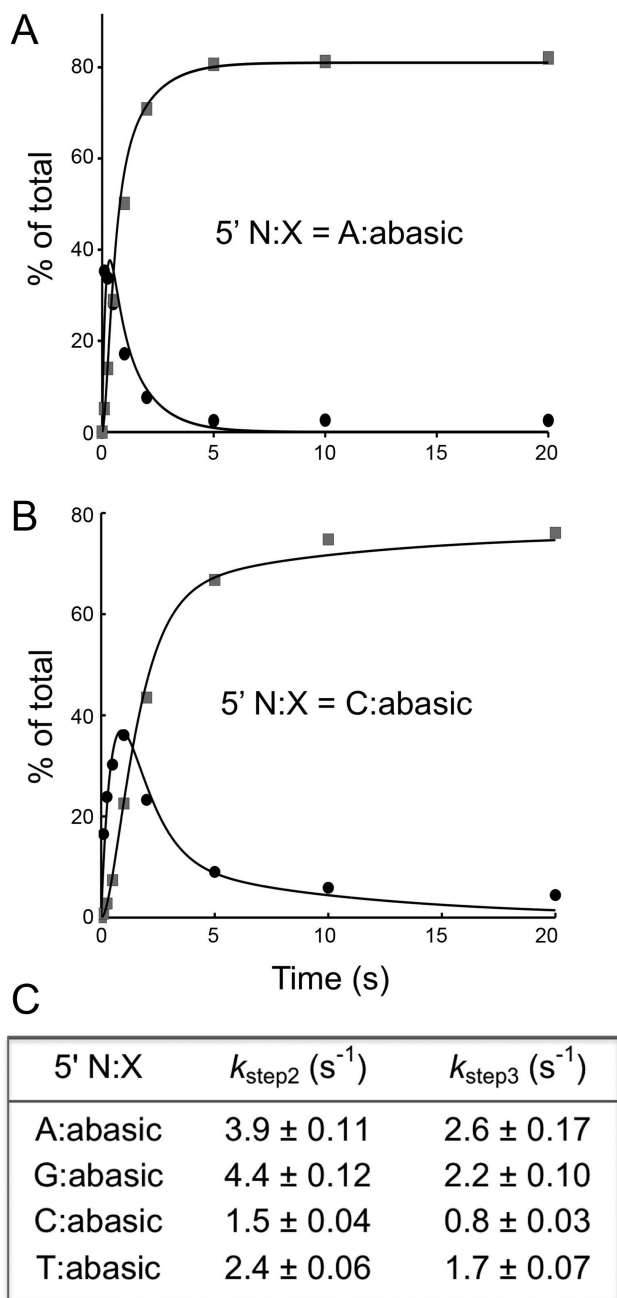
and 5′ T:abasic (k_{step2} 2.4 s^{-1}; k_{step3} 1.7 s^{-1}) nicks fell within a 3-fold range of one another (Figure 6C). Thus, in absolute terms, *Eco*LigA did not have a strong preference for sealing a particular 5′ N:abasic configuration.

In the case of the 5′ A:basic substrate, the k_{step2} of 3.9 s^{-1} was 7-fold slower than that of a paired 5′ A:T nick (27 s^{-1}) and was within the range of k_{step2} values for the mispaired 5′ A:C (5.7 s^{-1}) and 5′ A:A (1.1 s^{-1}) substrates. Similarly, the 5′ A:abasic k_{step3} of 2.6 s^{-1} was 6-fold slower than a paired 5′ A:T nick (14.5 s^{-1}) and was in the mid-range of k_{step3} values for the mispaired 5′ A:C (3.4 s^{-1}) and 5′ A:A (1.1 s^{-1}) nicks. The step 2 and step 3 rates for the 5′ G:abasic nick were 5-fold and 11-fold slower than for a paired 5′ G:C nick. The k_{step2} and k_{step3} values for the 5′ C:abasic nick were 14-fold and 51-fold slower than for a paired 5′ C:G nick. The k_{step2} and k_{step3} values for the 5′ T:abasic nick were 3-fold and 5-fold slower than for a paired 5′ C:G nick. In general, the

effects of 5′ N:abasic lesions were in line with the effects of 5′ N:X mispairs.

We found that N:abasic sites on the 3′-OH side of the nick were far more deleterious than the equivalent 5′ N:abasic sites (Figure 7B). As was the case for the 3′ N:X mispairs, the kinetic profiles for sealing the 3′ N:abasic substrates could not be fit to the scheme used to derive step 2 and step 3 rate constants. For example, in the reaction at the 3′ G:abasic nick, AppDNA accumulated steadily over the first 4 min and plateaued at 6 to 30 min comprising 48–52% of total DNA (Figure 7A). Ligated DNA plateaued at 33% of total DNA at 20–30 min. This pattern suggests that a significant fraction of the AppDNA was rendered non-ligatable, perhaps because LigA had irreversibly dissociated from the 5′ adenylylated nick after step 2 catalysis. By fitting AppDNA plus ligated DNA to a single exponential, we derived k_{step2} of 0.007 s^{-1} for the 3′ G:abasic substrate, which

A

5' N:X = A:abasic

B

5' N:X = C:abasic

C

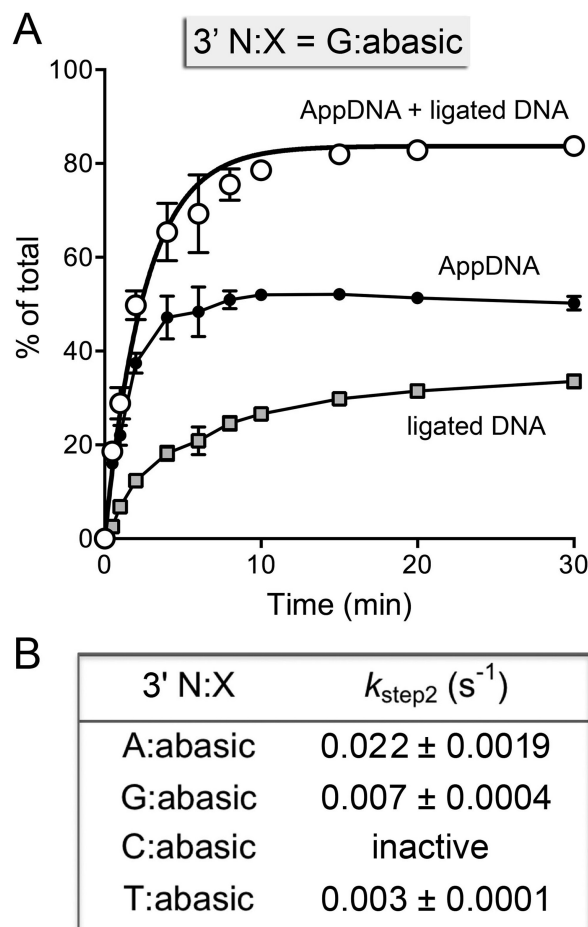| 5' N:X	k_{step2} (s^{-1})	k_{step3} (s^{-1})
A:abasic	3.9 ± 0.11	2.6 ± 0.17
G:abasic	4.4 ± 0.12	2.2 ± 0.10
C:abasic	1.5 ± 0.04	0.8 ± 0.03
T:abasic	2.4 ± 0.06	1.7 ± 0.07

Figure 6. Sealing of nicks with 5′ N:abasic lesions. (**A and B**) The distributions of radiolabeled AppDNA intermediate (black circles) and ligated 36-mer DNA product (gray squares) during the reaction of *Eco*LigA–AMP at the 5′ A:abasic nick (panel A) and the 5′ C:abasic nick (panel B) are plotted as a function of time. The curve fits to the kinetic scheme are shown. (**C**) The step 2 and step 3 rate constants for sealing nicks with the indicated 5′ N:abasic configurations are shown.

A

3' N:X = G:abasic

B

3' N:X	k_{step2} (s^{-1})
A:abasic	0.022 ± 0.0019
G:abasic	0.007 ± 0.0004
C:abasic	inactive
T:abasic	0.003 ± 0.0001

Figure 7. Sealing of nicks with 3′ N:abasic lesions. (**A**) The distributions (±SEM) of radiolabeled AppDNA intermediate (black circles), ligated 36-mer DNA product (gray squares) and the sum of AppDNA plus ligated DNA (open circles) during the reaction of *Eco*LigA–AMP at the 3′ G:abasic nick are plotted as a function of time. The thick black curve though the open circles shows the nonlinear regression fit of the sum of AppDNA plus ligated DNA to a single exponential, from which we derived k_{step2}. (**B**) The step 2 rate constants for sealing nicks with the indicated 3′ N:abasic configurations are shown. The 3′ C:abasic nick was deemed inactive by the criterion than there was no detectable formation of AppDNA or ligated DNA during a 40 min reaction with *Eco*LigA–AMP.

ure 7B). The C:abasic lesion was more deleterious than any of the 3′ C:X mispairs (Figure 5E). The 3′ A:abasic nick was the favored substrate of the 3′ N:abasic series, with a step 2 rate constant of 0.022 s^{-1} (Figure 7B), this being 7-fold and 11-fold faster than k_{step2} at the 3′ A:C and 3′ A:A mispairs (Figure 5E).

Effects of 3′ N:oxoguanine lesions on the kinetics of nick sealing

Oxidative damage to DNA generates 8-oxoguanine (oxoG). The effects and metabolism of oxoG in DNA have been studied intensively in light of its mutagenic properties, which ensue from the ability of oxoG in the *syn* nucleoside conformation to mispair with adenine (see Figure 8B). This pairing prompts DNA polymerases to embed A:oxoG mispairs, which can ultimately lead to G→T transversions

was 1300-fold slower than k_{step2} at a paired 3′ G:C nick, but was similar to k_{step2} of 0.006 s^{-1} at a 3′ G:T mispair.

The k_{step2} value for the 3′ T:abasic nick was 0.003 s^{-1}, which was similar to k_{step2} value for the 3′ T:T mispaired nick (0.004 s^{-1}). The 3′ C:abasic nick was inactive, insofar as there was no detectable formation of AppDNA or ligated DNA during a 40 min reaction with *Eco*LigA–AMP (Fig-
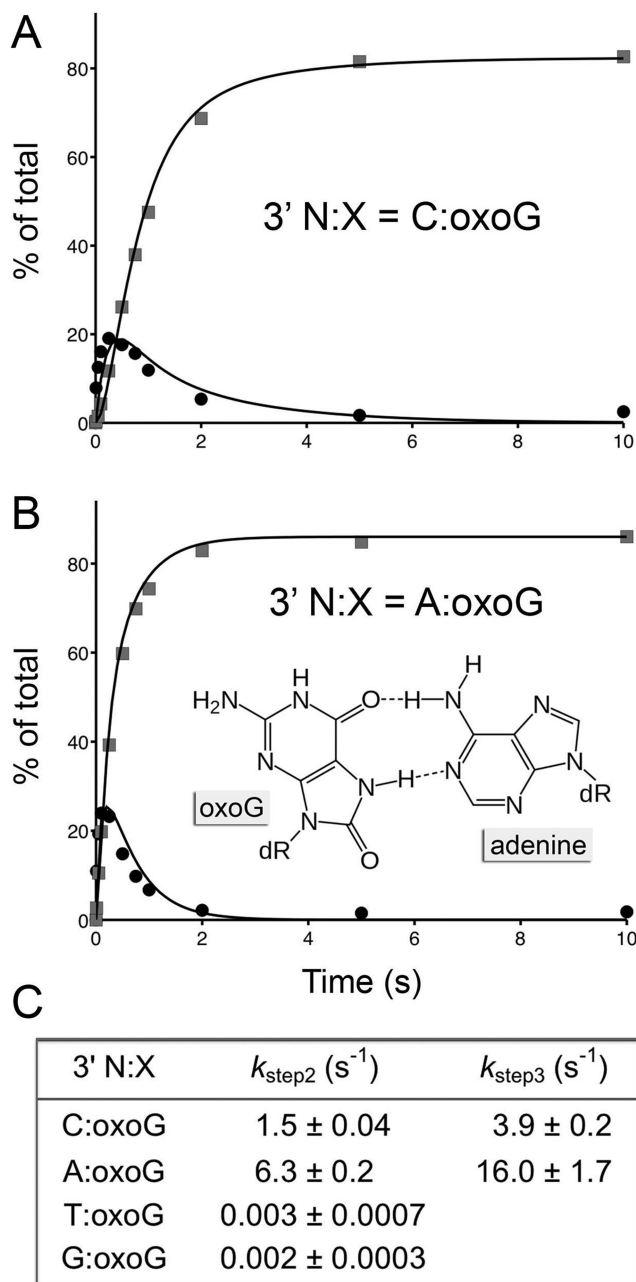
Figure 8. Sealing of nicks with 3′ N:oxoguanine lesions. (**A** and **B**) The distributions of radiolabeled AppDNA intermediate (black circles) and ligated 36-mer DNA product (gray squares) during the reaction of *Eco*LigA–AMP at the 3′ C:oxoG nick (panel A) and the 3′ A:oxoG nick (panel B) are plotted as a function of time. The curve fits to the kinetic scheme are shown. The chemical structure of the A:oxoG pair with oxoG in the *syn* conformation is shown as an inset in panel B; hydrogen-bonding contacts are indicated by dashed lines. (**C**) The step 2 and step 3 rate constants for sealing nicks with the indicated 3′-OH N:oxoG configurations are shown.

if not corrected. Were polynucleotide ligases to seal mispairs at oxoG in the template strand, this would also be pro-mutagenic. There have been reports of oxopurine effects on T4 and human DNA ligases (50,51) and T4 RNA ligase 2 (36).

Here, we determined the transient-state kinetics of *Eco*LigA in sealing nicked duplexes with oxoG in the template strand opposite the 3′-OH deoxynucleotide at the nick. By testing all N:oxoG pairs and the comparing the rate constants for sealing these damaged substrates to the rates for the corresponding undamaged N:G substrates, we aimed to discern whether certain damaged configurations are more or less prone to sealing by *Eco*LigA.

The kinetic profiles for sealing of the 3′ C:oxoG and 3′ A:oxoG substrates are shown in Figure 8A,B. The apparent step 2 and step 3 rate constants of 1.5 s^{-1} and 3.9 s^{-1} for the 3′ C:oxoG nick (Figure 8C) were reduced by 15-fold and 11-fold, respectively, compared with those for a canonical 3′ C:G pair. The salient finding was that the 3′ A:oxoG was a much better substrate for *Eco*LigA, with k_{step2} of 6.3 s^{-1} and k_{step3} of 16.0 s^{-1} (Figure 8C), which were in the range of a correctly paired nick, and were in stark contrast to the inactivity of *Eco*LIgA at a mispaired 3′ A:G nick (Figure 5E). Thus, a key consequence of oxoG in the template strand across from the nick 3′-OH is to enable the embedding by *Eco*LigA of dAMP in lieu of dCMP at the repair junction.

A different scenario applied to the 3′ T:oxoG and 3′ G:oxoG nicks, which behaved as typical 3′ N:X mispairs that severely compromised ligation, by slowing the overall kinetics and accumulating high levels of AppDNA (28% and 54% of total DNA for 3′ T:oxoG and 3′ G:oxoG, respectively) that persisted at 20–40 min reaction times. From the sum of AppDNA plus ligated DNA versus time, we derived k_{step2} values of 0.003 s^{-1} for 3′ T:oxoG and 0.002 s^{-1} for 3′ G:oxoG (Figure 8C).

CONCLUSIONS AND IMPLICATIONS

Here we elucidated the kinetic mechanism of single-turnover nick sealing by *Eco*LigA–AMP and determined the effects of base mispairs and base damage lesions on the rates of nick 5′-adenylylation and phosphodiester synthesis. The pertinent findings with respect to the sealing of perfectly paired nicks were that the rates of step 2 catalysis were rapid (6.8–27 s^{-1}) and similar in magnitude to the step 3 rates (8.3–42 s^{-1}). To our knowledge, this is the first transient state kinetic analysis of a LigA–AMP enzyme. Our finding adds to existing steady-state kinetic studies of the NAD$^+$-dependent nick joining reactions of *Eco*LigA and *Haemophilus influenzae* LigA, both of which are stimulated strongly by ammonium sulfate (37,52,53). We found that ammonium ion enhances the rate of step 2 and step 3 catalysis by *Eco*LigA–AMP, as much as 53-fold and 20-fold, respectively, at 15 mM ammonium sulfate. The structural basis for the ammonium effect on steps 2 and 3 remains unclear. It is conceivable that ammonium promotes the DNA conformational changes induced by LigA binding or directly affects the LigA active site (16).

Our analysis of ligase fidelity highlighted that *Eco*LigA was exquisitely kinetically sensitive to all 3′-OH base mispairs and 3′ N:abasic lesions, but comparatively tolerant of 5′-PO$_4$ mispairs and 5′ N:abasic sites. The consistent and instructive results were that 3′ N:X fidelity was enforced at the level of step 2 catalysis, whereby 3′ N:X mispairs slowed 5′ adenylylation by three to four orders of magnitude or, in the case of the 3′ A:G, 3′ G:A and 3′ C:abasic nicks, rendered

the substrate inert. We surmise that *Eco*LigA is acutely dependent on proper positioning of the 3′ terminal nucleoside to attain optimal rates of 5′ adenylylation, and that the mispair effects on step 2 rate reflect the degree to which the nick is structurally perturbed. This view is consistent with prior studies showing that: (i) there is a network of functionally important atomic contacts of *Eco*LigA with the 3′-OH side of the nick (16,18–20); and (ii) replacing the terminal 3′-OH at the nick with a 3′-H slows step 2 by a factor of 1000, even though the 3′-OH is not chemically transformed during the step 2 reaction (37).

Step 3 catalysis was also affected by 3′ N:X mispairs and 3′ N:abasic sites, as evinced by the accumulation and persistence of AppDNA that was not ligated when an apparent reaction endpoint had been attained. One simple explanation for this behavior is that certain 3′ N:X configurations predispose *Eco*LigA to dissociate from AppDNA after step 2 catalysis and then do not allow for rebinding by LigA apoenzyme. Alternatively, *Eco*LigA might remain at the 3′N:X/AppDNA nick after step 2, but fall into an off-pathway conformation that is durably inactive for phosphodiester formation.

Our evaluation of the effects of oxoguanine in the template strand opposite the nick 3′-OH underscored the importance of a correctly positioned 3′-OH nucleotide for nick sealing by *Eco*LigA, evident in the 'gain-of function' seen for a 3′ A:oxoG Hoogsteen configuration that *Eco*LigA readily accepted as a correctly paired end for rapid sealing, while discriminating powerfully against sealing 3′ T:oxoG and 3′ G:oxoG mispairs. The activity of *Eco*LigA at the 3′ A:oxoG nick is in tune with the pro-mutagenic properties of certain DNA polymerases that copy over template oxoG sites to generate A:oxoG configurations (54). *E. coli* and many other bacteria have a MutY glycosylase that excises the A nucleobase at an A:oxoG pair to yield an abasic:oxoG lesion, which then undergoes incision and removal of the abasic site, single-nucleotide gap filling by a polymerase to form a 3′ C:oxoG (or 3′ A:oxoG) nick, and subsequent ligation (55). [A 3′ C:oxoG product can undergo a second round of base excision repair by the MutM glycosylase, which removes the oxoG base (55).] Our data indicate that *Eco*LigA–AMP is faster at sealing the 3′ A:oxoG nick than the 3′ C:oxoG nick under single-turnover conditions. Thus, it is plausible for LigA to embed a mutagenic A:oxoG lesion at a nick during DNA repair (in effect, making a futile cycle with MutY).

High-fidelity thermophilic NAD$^+$-dependent DNA ligases have been used to develop detection/amplification methods for molecular diagnostics, including the detection of single-nucleotide polymorphisms and disease-associated mutations (55-57). Luo *et al.* (41) assessed initial rates of nick sealing by *Thermus thermophilus* (*Tth*) LigA at all combinations of paired and mispaired 3′N:X nicks under steady-state conditions and found that only 3′ T:G and 3′ G:T nicks were detectably sealed. They reported fidelity values (ratio of paired 3′ N:X rate to mispaired 3′ N:X rate) in the range of 450–1500 for the 3′ T:G mispair. We find that *Eco*LigA–AMP has a fidelity value of 2800 for a 3′ T:G nick, based on the k_{step2} ratio. Thus, *Eco*LigA is suitable in principle for ligase-based detection methods that do not require iterative thermocyling.

REFERENCES

1. Shuman,S. (2009) DNA ligases: progress and prospects. *J. Biol. Chem.*, **294**, 17365–17369.
2. Sriskanda,V., Moyer,R.W. and Shuman,S. (2001) NAD$^+$-dependent DNA ligase encoded by a eukaryotic virus. *J. Biol. Chem.*, **276**, 36100–36109.
3. Zhao,A, Gray,F.C. and MacNeill,S.A. (2006) ATP- and NAD$^+$-dependent DNA ligases share an essential function in the halophilic archaeon *Haloferax volcanii. Mol. Microbiol.*, **59**, 743–752.
4. Poidevin,L. and MacNeill,S.A. (2006) Biochemical characterization of LigN, an NAD$^+$-dependent DNA ligase from the halophilic euryarchaeon *Haloferax volcanii* that displays maximal *in vitro* activity at high salt concentrations. *BMC Mol. Biol.*, **7**, 44.
5. Benarroch,D. and Shuman,S. (2006) Characterization of mimivirus NAD$^+$-dependent DNA ligase. *Virology*, **353**, 133–143.
6. Ellenberger,T. and Tomkinson,A.E. (2008) Eukaryotic DNA ligases: structural and functional insights. *Annu. Rev. Biochem.*, **77**, 313–338.
7. Olivera,B.M. and Lehman,I.R. (1967) Linkage of polynucleotides through phosphodiester bonds by an enzyme from *Escherichia coli. Proc. Natl. Acad. Sci. U.S.A.*, **57**, 1426–1433.
8. Olivera,B.M. and Lehman,I.R. (1967) Diphosphopyridine nucleotide: a cofactor for the polynucleotide-joining enzyme from *Escherichia coli. Proc. Natl. Acad. Sci. U.S.A.*, **57**, 1700–1704.
9. Olivera,B.M., Hall,Z.W. and Lehman,I.R. (1968) Enzymatic joining of polynucleotides, V: a DNA-adenylate intermediate in the polynucleotide-joining reaction. *Proc. Natl. Acad. Sci. U.S.A.*, **61**, 237–244.
10. Gellert,M. (1967) Formation of covalent circles of lambda DNA by *E. coli* extracts. *Proc. Natl. Acad. Sci. U.S.A.*, **57**, 148–155.
11. Zimmerman,S.B., Little,J.W., Oshinsky,C.K. and Gellert,M. (1967) Enzymatic joining of DNA strands: a novel reaction of diphosphopyridine nucleotide. *Proc. Natl. Acad. Sci. U.S.A.*, **57**, 1841–1848.
12. Little,J.W., Zimmerman,S.B., Oshinsky,C.K. and Gellert,M. (1967) Enzymatic joining of DNA strands, II: an enzyme-adenylate intermediate in the DPN-dependent DNA ligase reaction. *Proc. Natl. Acad. Sci. U.S.A.*, **58**, 2004–2011.
13. Gumport,R.I. and Lehman,I.R. (1971) Structure of the DNA ligase-adenylate intermediate: lysine (ε-amino)-linked adenosine monophosphoramidate. *Proc. Natl. Acad. Sci. U.S.A.*, **68**, 2559–2563.
14. Gajiwala,K. and Pinko,C. (2004) Structural rearrangement accompanying NAD$^+$ synthesis within a bacterial DNA ligase crystal. *Structure*, **12**, 1449–1459.
15. Sriskanda,V. and Shuman,S. (2002) Conserved residues in domain Ia are required for the reaction of *Escherichia coli* DNA ligase with NAD$^+$. *J. Biol. Chem.*, **277**, 9685–9700.
16. Nandakumar,J., Nair,P.A. and Shuman,S. (2007) Last stop on the road to repair: structure of *E. coli* DNA ligase bound to nicked DNA-adenylate. *Mol. Cell*, **26**, 257–271.
17. Sriskanda,V., Schwer,B., Ho,C.K. and Shuman,S. (1999) Mutational analysis of *E. coli* DNA ligase identifies amino acids required for nick-ligation *in vitro* and for *in vivo* complementation of the growth of yeast cells deleted for *CDC9* and *LIG4. Nucleic Acids Res.*, **27**, 3953–3963.
18. Zhu,H. and Shuman,S (2005) Structure-guided mutational analysis of the nucleotidyltransferase domain of *Escherichia coli* NAD$^+$-dependent DNA Ligase (LigA). *J. Biol. Chem.*, **280**, 12137–12144.
19. Wang,L.K., Nair,P.A. and Shuman,S. (2008) Structure-guided mutational analysis of the OB, HhH and BRCT domains of *Escherichia coli* DNA ligase. *J. Biol. Chem.*, **283**, 23343–23352.
20. Wang,L.K., Zhu,H. and Shuman,S (2009) Structure-guided mutational analysis of the nucleotidyltransferase domain of *Escherichia coli* DNA Ligase (LigA). *J. Biol. Chem.*, **284**, 8486–8494.
21. Odell,M., Sriskanda,V., Shuman,S. and Nikolov,D. (2000) Crystal structure of eukaryotic DNA ligase–adenylate illuminates the

mechanism of nick sensing and strand joining. *Mol. Cell*, **6**, 1183–1193.

22. Sriskanda,V. and Shuman,S. (2002) Role of nucleotidyl transferase motif V in strand joining by *Chlorella* virus DNA ligase. *J. Biol. Chem.*, **277**, 9661–9667.

23. Sriskanda,V. and Shuman,S. (2002) Role of nucleotidyl transferase motifs I, III and IV in the catalysis of phosphodiester bond formation by *Chlorella* virus DNA ligase. *Nucleic Acids Res.*, **30**, 903–911.

24. Nair,P.A., Nandakumar,J., Smith,P., Odell,M., Lima,C.D. and Shuman,S. (2007) Structural basis for nick recognition by a minimal pluripotent DNA ligase. *Nature Struct. Mol. Biol.*, **14**, 770–778.

25. Samai,P. and Shuman,S. (2011) Functional dissection of the DNA interface of the nucleotidyltransferase domain of *Chlorella* virus DNA ligase. *J. Biol. Chem.*, **286**, 13314–13326.

26. Samai,P. and Shuman,S. (2011) Structure-function analysis of the OB and latch domains of *Chlorella* virus DNA ligase. *J. Biol. Chem.*, **286**, 22642–22652.

27. Samai,P. and Shuman,S. (2012) Kinetic analysis of DNA strand joining by *Chlorella* virus DNA ligase and the role of nucleotidyltransferase motif VI in ligase adenylylation. *J. Biol. Chem.*, **287**, 28609–28618.

28. Ho,C.K. and Shuman,S. (2002) Bacteriophage T4 RNA ligase 2 (gp24.1) exemplifies a family of RNA ligases found in all phylogenetic domains. *Proc. Natl. Acad. Sci. U.S.A.*, **99**, 12709–12714.

29. Yin,S., Ho,C.K. and Shuman,S. (2003) Structure-function analysis of T4 RNA ligase 2. *J. Biol. Chem.*, **278**, 17601–17608.

30. Ho,C.K., Wang,L.K., Lima,C.D. and Shuman,S. (2004) Structure and mechanism of RNA ligase. *Structure*, **12**, 327–339.

31. Nandakumar,J., Ho,C.K., Lima,C.D. and Shuman,S. (2004) RNA substrate specificity and structure-guided mutational analysis of bacteriophage T4 RNA ligase 2. *J. Biol. Chem.*, **279**, 31337–31347.

32. Nandakumar,J. and Shuman,S. (2004) How an RNA ligase discriminates RNA versus DNA damage. *Mol. Cell*, **16**, 211–221.

33. Nandakumar,J. and Shuman,S. (2005) Dual mechanisms whereby a broken RNA end assists the catalysis of its repair by T4 RNA ligase 2. *J. Biol. Chem.*, **280**, 23484–23489.

34. Taylor,M.R., Conrad,J.A., Wahl,D. and O'Brien,P.J. (2011) Kinetic mechanism of human DNA ligase I reveals magnesium-dependent changes in the rate-limiting step that compromise ligation efficiency. *J. Biol. Chem.*, **286**, 23054–23062.

35. Lohman,G.S., Chen,L. and Evans,T.C. (2011) Kinetic characterization of single strand break ligation in duplex DNA by T4 DNA ligase. *J. Biol. Chem.*, **286**, 44187–44196.

36. Chauleau,M. and Shuman,S. (2013) Kinetic mechanism of nick sealing by T4 RNA ligase 2 and effects of 3'-OH base mispairs and damaged base lesions. *RNA*, **19**, 1840–1847.

37. Modrich,P and Lehman,I.R. (1973) Deoxyribonucleic acid ligase: a steady state kinetic analysis of the reaction catalyzed by the enzyme from *Escherichia coli*. *J. Biol. Chem.*, **248**, 7502–7511.

38. Tomkinson,A.E., Tappe,N.J. and Friedberg,E.C. (1992) DNA ligase I from *Saccharomyces cerevisiae*: physical and biochemical characterization of the CDC9 gene product. *Biochemistry*, **31**, 11762–11771.

39. Husain,I., Tomkinson,A.E., Burkhart,W.A., Moyer,M.B., Ramos,W., Mackey,Z.B., Besterman,J.M. and Chen,J. (1995) Purification and characterization of DNA ligase III from bovine testes: homology with DNA ligase II and vaccinia DNA ligase. *J. Biol. Chem.*, **270**, 9683–9690.

40. Shuman,S. (1995) Vaccinia virus DNA ligase: specificity, fidelity, and inhibition. *Biochemistry*, **34**, 16138–16147.

41. Luo,J., Bergstrom,D.E. and Barany,F. (1996) Improving the fidelity of *Thermus thermophilus* DNA ligase. *Nucleic Acids Res.*, **24**, 3071–3078.

42. Sriskanda,V. and Shuman,S. (1998) Specificity and fidelity of strand joining by *Chlorella* virus DNA ligase. *Nucleic Acids Res.*, **26**, 3536–3541.

43. Bhagwat,A.A., Sanderson,R.J. and Lindahl,T. (1999) Delayed DNA joining at 3' mismatches by human DNA ligases. *Nucleic Acids Res.*, **27**, 4028–4033.

44. Tong,J., Barany,F. and Cao,W. (2000) Ligation reaction specificities of an NAD$^+$-dependent DNA ligase from the hypethermophile *Aquifex aeolicus*. *Nucleic Acids Res.*, **28**, 1447–1454.

45. Nakatani,M., Ezaki,S., Atomi,H. and Imanaka,T. (2002) Substrate recognition and fidelity of strand joining by an archaeal DNA ligase. *Eur. J. Biochem.*, **269**, 650–656.

46. Lamarche,B.J., Showalter,A.K. and Tsai,M.D. (2005) An error-prone viral DNA ligase. *Biochemistry*, **44**, 8408–8417.

47. Wang,Y., Lamarche,B.J. and Tsai,M.D. (2007) Human DNA ligase IV and the ligase IV/XRCC4 complex: analysis of nick ligation fidelity. *Biochemistry*, **46**, 4962–4976.

48. Kim,J. and Mrksich,M. (2010) Profiling the selectivity of DNA ligases in an array format with mass spectrometry. *Nucleic Acids Res.*, **38**, e2.

49. Lohman,G.J., Bauer,R.J., Nichols,N.M., Mazzola,L., Bybee,J., Rivizzigno,D., Cantin,E. and Evans,TC. (2016) A high-throughput assay for the comprehensive profiling of DNA ligase fidelity. *Nucleic Acids Res.*, **44**, e14.

50. Hashimoto,K., Tominaga,Y., Nakabeppu,Y. and Moriya,M. (2004) Futile short-patch DNA base excision repair of adenine:8-oxoguanine mispair. *Nucleic Acids Res.*, **32**, 5928–5934.

51. Zhao,X., Muller,J.G., Halasyam,M., David,S.S. and Burrows,C.J. (2007) In vitro ligation of oligodeoxynucleotide containing C8-oxidized purine lesions using bacteriophage T4 DNA ligase. *Biochemistry*, **46**, 3734–3744.

52. Shapiro,A.B., Eakin,A.E., Walkup,G.K. and Rivin,O. (2011) A high-throughput fluorescence resonance energy transfer-based assay for DNA ligase. *J. Biomol. Screen.*, **16**, 486–493.

53. Shapiro,A.B. (2014) Complete steady-state rate equation for DNA ligase and its use for measuring product kinetic parameters of NAD$^+$-dependent DNA ligase from *Haemophilus influenza*. *BMC Res. Notes*, **7**, 287.

54. Zahn,K.E., Wallace,S.S. and Doublié,S. (2011) DNA polymerases provide a canon of strategies for translesion synthesis past oxidatively generated lesions. *Curr. Opin. Struct. Biol.*, **21**, 358–369.

55. De Oliveira,A.H., da Silva,A.E., de Oliveira,I.M., Henriques,J.A. and Agnez-Lima,L.F. (2014) MutY glycosylase: an overview on mutagenesis and activities beyond the GO system. *Mutat. Res.*, **769**, 119–131.

56. Barany,F. (1991) Genetic disease detection and DNA amplification using cloned thermostable ligase. *Proc. Natl. Acad. Sci. U.S.A.*, **88**, 189–193.

57. Li,J, Chu,X, Liu,Y, Jiang,JH, He,Z, Zhang,Z, Shen,G and Yu,R,Q. (2005) A colorimetric method for point mutation detection using high-fidelity DNA ligase. *Nucleic Acids Res.*, **33**, e168.